

Time-dependent Mechanical Properties and Structural Behaviour of Graphene Nanoplatelet-reinforced Concrete

Journal:	<i>Canadian Journal of Civil Engineering</i>
Manuscript ID	cjce-2024-0140.R1
Manuscript Type:	Research Article
Date Submitted by the Author:	23-Sep-2024
Complete List of Authors:	Yager, Jacob; Queen's University, Department of Civil Engineering, Smith Engineering Haridas, Haritha; Queen's University, Department of Chemical Engineering, Smith Engineering Woods, Joshua; Queen's University, Department of Civil Engineering, Smith Engineering Kontopoulou, Marianna; Queen's University, Department of Chemical Engineering, Smith Engineering
Is the manuscript for consideration in a Special Issue or Collection?:	Not applicable (regular submission)
Keyword:	Graphene nanoplatelets, Reinforced concrete, Early age concrete, Low carbon concrete, Distributed fibre optic sensors

SCHOLARONE™
 Manuscripts

1 **Time-dependent Mechanical Properties and Structural Behaviour**
2 **of Graphene Nanoplatelet-reinforced Concrete**

3 Jacob Yager^a, Haritha Haridas^b, Joshua E. Woods^c, and Marianna Kontopoulou^d

4 ^a Department of Civil Engineering, Smith Engineering, Queen's University, 58 University Ave.,
5 Kingston, On. Canada, K7L 3N6, 15jy36@queensu.ca (corresponding author)

6 ^b Department of Chemical Engineering, Smith Engineering, Queen's University, 19 Division St.,
7 Kingston, On. Canada, K7L 2N9, haritha.haridas@queensu.ca

8 ^c Department of Civil Engineering, Smith Engineering, Queen's University, 58 University Ave.,
9 Kingston, On. Canada, K7L 3N6, joshua.woods@queensu.ca

10 ^d Department of Chemical Engineering, Smith Engineering, Queen's University, 19 Division St.,
11 Kingston, On. Canada, K7L 2N9, kontopm@queensu.ca

12
13
14
15
16
17
18
19
20
21
22
23

Draft

24 Abstract

25 Concrete with low volumes of Portland cement often have lower early age compressive strength
26 and slower strength gain with time. It has been reported that the addition of graphene nanoplatelets
27 (GNPs) enhances concrete compressive strength. However, the ability of GNPs to increase the
28 early age concrete compressive strength has not been investigated, and there has been limited
29 testing of structural elements of GNP-containing concrete. This study examines the mechanical
30 properties of low cement concrete between 1- and 28-days of curing with varying GNP
31 concentrations. Furthermore, reinforced concrete beams with GNPs were tested at 3 and 28 days
32 to investigate their structural behaviour. The results show compressive strength increases of up to
33 31% at early ages for a GNP concentration of 0.15 wt% of cement, but no overall changes in the
34 structural behaviour.

35 **Keywords:** Graphene nanoplatelets; Reinforced concrete; Early age concrete; Low carbon
36 concrete; Distributed fibre optic sensors

37 **1.0 Introduction**

38 Cement is the second most used commodity worldwide, after only water (Chaudhury et al., 2023).
39 The production of cement, which is the main binding ingredient of concrete, generates about 7%
40 of global CO₂ emissions worldwide. In recent years, concrete mix designs have been altered to
41 increase the use of supplementary cementitious materials (SCM) and decrease the use of Portland
42 cement, and thus lowering the embodied carbon (Adesina, 2020). However, the use of SCMs and
43 decreased use of Portland cement in mix designs can result in slower compressive strength gain
44 over time when compared with traditional concrete mix designs. Slower concrete strength gain can
45 result in reduced construction efficiency (e.g., delays in removing formwork), which contributes
46 to hesitancy in the industry surrounding adoption of low carbon concrete (Kim et al., 2013). Thus,
47 there is a need for new concrete additives to improve the time-dependent strength gain of lower
48 carbon concrete.

49 One innovative solution to this challenge is the use of graphene nanoplatelets (GNPs).
50 GNPs consist of layers of graphene sheets. Their nanoscale dimensions and platelet structure result
51 in a large surface area and surface area-to-volume ratio. GNPs have many potential benefits
52 including high tensile strength, excellent thermal and electrical conductivity (Ismail et al., 2021),
53 and small environmental impact relative to other concrete additives (Jaramillo and Kalfat, 2023),
54 making them suitable for use in cementitious materials (Jiang et al., 2021). GNPs are also relatively
55 inexpensive compared to other nanomaterials (e.g., cost as low as \$450/kg) (Cheaptubes, 2023)
56 and small volumes (e.g., fractions of a percent by cement weight) are needed to observe maximum
57 benefits in the mechanical properties of concrete (Ismail et al., 2022), making it feasible for use
58 at-scale and in large-scale construction applications.

59 Researchers have studied the influence of GNPs in concrete for the purpose of exhibiting
60 self-sensing abilities (Al-Dahawi et al., 2016; Dai Pang et al., 2014; Sevim et al., 2022), improving
61 freeze-thaw resistance (Chen et al., 2019; Tong et al., 2016), enhanced prevention of water and
62 chloride ingress (Du et al., 2016; Du and Dai Pang, 2015; Zhang et al., 2022), and increased
63 durability through decreased carbonation depths under various climate conditions (Zhang et al.,
64 2021). Much of these benefits are the result of the ability of GNPs to provide lowered porosity,
65 and thus increased durability, through enhanced particle packing provided by the presence of the
66 GNP in the concrete matrix (Meng and Khayat, 2018). In addition to the durability enhancements
67 described above, enhanced mechanical properties from the addition of GNP (e.g., compressive or
68 tensile strength) could provide the most benefit for concrete mixes from a structural engineering
69 perspective, particularly at an early age (e.g, less than 7 days).

70 In recent years, there has been some investigation into the mechanical properties of GNP
71 mortar or cementitious composites (without coarse aggregate). Wang et al. (2016) found that
72 incorporation of GNPs enhanced the flexural strength of prisms by up to 24% and compressive
73 strength by up to 8%. Wang and Pang (2019) found compressive strength increases by up to 20%
74 through the incorporation of GNPs and Abedi et al. (2020) achieved up to 46% increases in
75 compressive strength and 43% increases in flexural strength with a combination GNP and carbon
76 nanotube reinforced cementitious composite.

77 There has also been some exploration into the effect of adding GNPs in concrete with
78 coarse aggregate, which would be more suitable for structural applications with reinforced
79 concrete. From the above literature, there have been mixed results on the degree to which GNPs
80 can enhance the mechanical properties of concrete and what GNP content provides optimal
81 performance. Table 1 summarizes the results of literature studies on the mechanical properties of

82 GNP concrete. Researchers have found a wide range of optimal GNP concentrations between
 83 0.025 and 0.25 wt% of cement that resulted in improved compressive strengths from anywhere
 84 between 17% to 146% (Dimov et al., 2018; Chen et al., 2019; Jiang et al. 2021; Ismail et al. 2022;
 85 Jaramillo and Kalfat 2023). Furthermore, researchers have also found improvements in flexural
 86 strength from 6% up to 70%. The large majority of these studies examined the material properties
 87 of the GNP concrete at 28 days after pouring. However, current construction practices typically
 88 require that temporary formworks be removed as early as one day after casting, meaning that a
 89 large portion of the 28-day concrete strength is required at that age, something that presents a
 90 challenge for low carbon concrete (with low amounts of Portland cement) which typically have
 91 much slower strength gain (Sahu and Shanmugapriya, 2022). Consequently, there is a need to
 92 better understand the effects of GNP addition on the early age strength of concrete as well as its
 93 effects on concrete mechanical properties at 28 days.

94 **Table 1:** Summary of studies focused on the use of GNP in concrete for mechanical property
 95 enhancement

Study	Cement Content (kg/m ³)	Water to Cement Ratio (w/c)	Optimum GNP Concentration (wt % cement)	Increase in Compressive Strength	Increase in Flexural Strength
Dimov et al. (2018)	n/a	0.57	0.04%	146%	80%
Chen et al. (2019)	n/a	0.6	0.05%	22%	n/a
Jiang et al. (2021)	433.1	0.5	0.025-0.075%	17%	6%
Ismail et al. (2022)	500	0.33	0.02%	21%	13%
Divya et al. (2023)	345	0.4	0.25%	40%	70%
Jaramillo and Kalfat (2023)	290	0.6	0.25%	20%	9%

96
 97 Despite the above research into the mechanical properties, there has been limited investigation into
 98 the structural behaviour of GNP and steel reinforced concrete. Only Ismail et al. (2022) tested
 99 GNP concrete reinforced with steel. However, in each of those specimens the steel reinforcement

100 was designed to yield, which means that the beam behaviour was governed by the behaviour of
101 the steel reinforcement, rather than the concrete (and the influence of the GNPs). However, this
102 study did demonstrate that low dosages of GNPs (up to 0.1 wt% of cement) resulted in higher first
103 cracking load, yielding load, and ultimate load, albeit in a limited sample size.

104 Based on this assessment of the literature, the overarching aim of this study is to assess the
105 effectiveness of GNPs as an additive for concrete with low amounts of Portland cement by: (i)
106 quantifying the compressive strength and modulus of rupture for a range of GNP dosages, (ii)
107 measuring the time-dependent compressive strength of the GNP concrete, and (iii) evaluating the
108 structural behaviour of GNP and steel rebar reinforced concrete beams through the use of
109 distributed sensing at 3 and 28 days after casting.

110 **2.0 Materials and Methods**

111 **2.1 Materials and Mixing Procedure**

112 Table 2 shows the concrete mix design, which was a modified mix based on low Portland cement
113 mixes recommended by Soutsos et al. (2017). The mix design contained relatively low amounts
114 of Portland cement when compared to a more traditional concrete mix design to examine the
115 effects of adding GNPs to a low Portland cement mix. The cement used in this study was high
116 early Portland cement (type HE) and the coarse aggregate had a maximum size of 14 mm. High
117 early cement was used in order to simulate a scenario in which early age strength is needed out of
118 a low cement mix while evaluating the ability of GNP to further enhance the early age strength.

119

120

121

122

Table 2: Concrete mix design

Ingredient	Density (kg/m³)
Water (w)	158
Cement (c)	285
Coarse Aggregate	1102
Fine Aggregate	799
GNP	Varies
w/c	0.55

123 While the contents of water, cement, coarse and fine aggregates remained consistent throughout
124 each set of specimens, the amount of GNPs varied depending on the concrete mix design, which
125 included GNP ratios by cement weight of 0.04 wt%, 0.07 wt%, 0.1 wt%, 0.15 wt%, 0.3 wt%, and
126 1 wt%. Table 3 shows the properties of the GNPs used in this study. The GNPs were manufactured
127 using a novel thermomechanical exfoliation approach proposed by Mardlin et al. (2022), which
128 includes elevated temperatures and mechanical shear force generated by two counterrotating
129 rotors. This method is not only environmentally friendly since it is solvent-free, but also scalable
130 as it can create large quantities of GNPs using commercially available equipment. This method
131 was later modified by Haridas et al. (2024), who employed a non-covalent functionalization
132 process that uses trimellitic anhydride to make the GNPs dispersible in water, a property that is
133 also required for dispersion in concrete. As shown in Table 3, the GNP product has a large variance
134 in flake sizes, which could lead to enhanced particle packing efficiency and thus, improved
135 porosity and mechanical properties in concrete. Additional information on the GNP particles used
136 in this study can be found in Haridas et al. (2024).

137

138

139

Table 3: Graphene nanoplatelet properties

Property	Value
Surface Area (m ² /g)	363 ± 11
Diameter (µm)	0.05-2
Thickness (nm)	1-25
Density (g/cm ³)	2.26
Carbon Content (%)	94.8

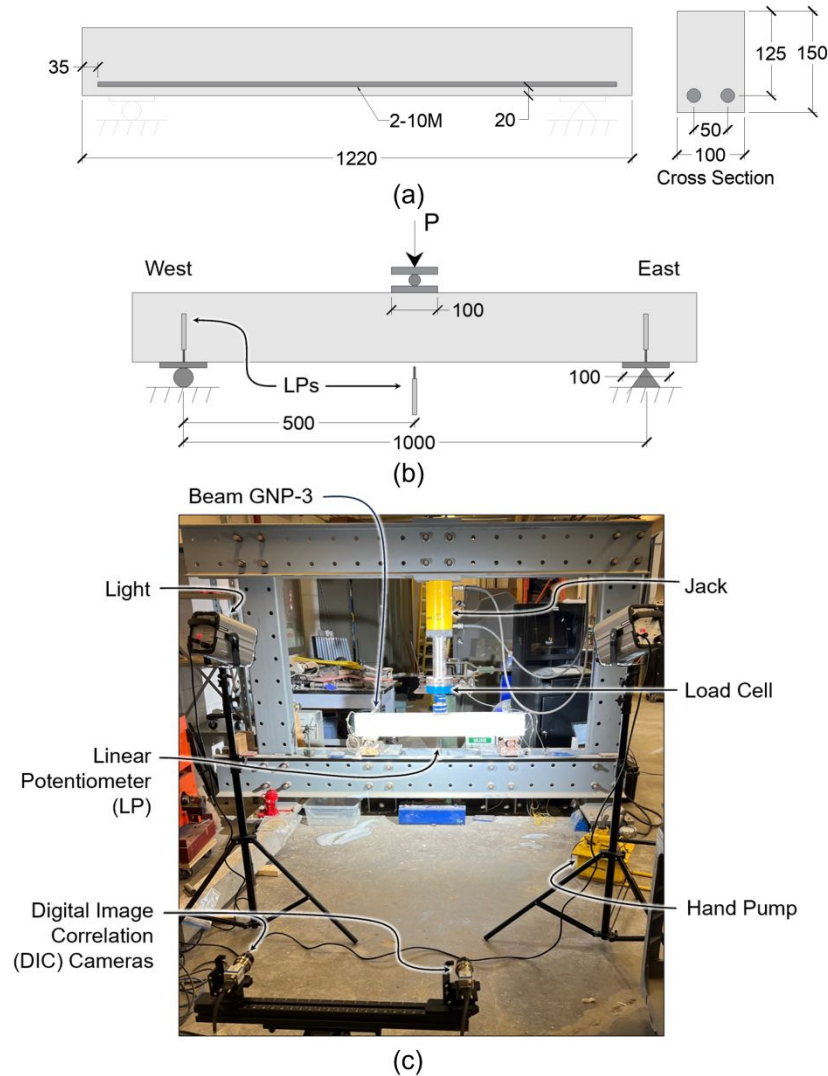
140 In this study, to ensure the stability and dispersion of the GNPs during the concrete mixing process,
 141 the water and GNPs were combined before being added to the concrete using a Silverson L4RT
 142 high shear mixer operated at a rotating speed of 5000 rpm for two hours, as described by Dimov
 143 et al. (2018). This was done for all mixtures, except for the composition containing 1 wt% of
 144 cement GNP. The 1 wt% GNP concrete was not shear mixed to investigate if the aggregation of
 145 GNPs that have not been wet dispersed affect the concrete mechanical properties. After dispersing
 146 the GNPs in the water, the concrete was mixed in a high shear concrete mixer by first adding the
 147 aggregates, followed by alternating volumes of water-GNP mixture and cement until all the
 148 materials were combined. There was little observed effect of the GNP on the concrete workability.

149 2.2 Test Specimens

150 Compressive strength and modulus of rupture (flexural strength) tests were conducted to
 151 investigate the time-dependent compressive strength of concrete with different concentrations of
 152 GNPs, as well as mechanical properties of the concrete at 28 days after pouring. Compressive
 153 strength was tested on 76 mm diameter × 150 mm long cylinders according to the procedures
 154 outlined in ASTM C39 (ASTM, 2021). Tests were completed 28 days after pouring for each of the
 155 GNP ratios, and additionally at 1, 3 and 7 days for the specimens containing 0.1 wt% and 0.15
 156 wt% GNPs. The GNP concentrations tested at early ages were chosen as they represented the
 157 highest potential based on compressive testing at 28-days. Flexural strength was measured through

158 testing of $76 \times 76 \times 285$ mm ($h \times w \times l$) prism specimens in four-point bending according to the
159 procedures outlined in ASTM C78 (ASTM, 2022). Each of these tests were completed at 28 days
160 after pouring.

161 In addition to testing the mechanical properties of the concrete, the structural behaviour
162 was also evaluated through testing of small-scale reinforced concrete beam specimens. Figure 1(a)
163 shows the configuration of the beams, which measured $150 \times 100 \times 1220$ mm ($h \times w \times l$) and had 2-
164 10M steel reinforcing bars at an effective depth (d) of 125 mm. The size of these specimens was
165 limited by the amount of GNP that could be feasibly produced given the production setup. Based
166 on testing of three coupons according to the procedures described in ASTM A370 (ASTM, 2023),
167 the rebar had an average tensile strength of 453 MPa (coefficient of variation (COV) = 1.2%). The
168 clear cover to the steel reinforcement at the bottom, ends, and sides of the beam were 20 mm, 35
169 mm, and 20 mm, respectively. Four beam specimens were tested: (1) beam C-3, which was
170 fabricated of high-early Portland cement concrete and was tested 3 days after curing, (2) beam C-
171 28, which was fabricated of high-early Portland cement concrete and was tested at 28 days after
172 curing, (3) beam GNP-3, which had 0.15 wt% GNP (by cement weight) concrete and was tested
173 at 3 days after curing, and (4) beam GNP-28, which had 0.15 wt% GNP (by cement weight)
174 concrete and was tested at 28 days after curing. The 0.15 wt% concentration of GNPs was used
175 because it was determined to be the optimal GNP concentration based on the results of the initial
176 material tests (i.e., compressive strength and modulus of rupture).



177

178 **Figure 1:** Specimen and test setup: (a) Geometry of beam specimens, (b) Geometry of beam test
 179 setup, (c) Beam test setup in lab (beam GNP-3 shown)

180 2.3 Instrumentation

181 To analyze the structural behaviour of the reinforced concrete beams, distributed sensing,
 182 including digital image correlation (DIC) and distributed fibre optic sensing (DFOS) were used.
 183 DIC involves the use of digital images to track displacements, strains, and concrete crack widths
 184 over the surface of a structural member. Several researchers have used DIC to track crack patterns

185 or measure crack widths and slips (Fayyad and Lees, 2014; Hoult et al., 2016; Yager et al., 2022a).
186 DFOS involves the use of a fibre optic cable bonded to a structural element (the internal steel
187 reinforcement in the beams in this study) and a laser is then used to measure the change in
188 wavelength of backscattered light, which is then converted to strain along the length of the fibre
189 (Masoudi and Newson, 2016). In experiments on reinforced concrete members, DFOS have been
190 used to measure distributed strains along the internal steel reinforcement (Yager et al., 2021) as
191 well as on the surface of the concrete (Villalba and Casas, 2013). Measurements have been used
192 to determine member deflections and curvatures (Brault and Hoult, 2019a), restrained concrete
193 shrinkage (Yager et al., 2022b), and force mechanisms in reinforced concrete (Poldon et al., 2022).

194 In this study, the surface of each beam specimen was painted with a black and white speckle
195 pattern prior to testing for DIC measurements. Figure 1 shows the configuration of the cameras.
196 Two cameras (to enable stereo vision) were used to take pictures of surface of the beam during
197 testing at a sampling rate of 1 Hz. The images were analyzed using the VIC-3D software
198 (Correlated Solutions Inc., 2023).

199 The beam specimens were also instrumented with nylon coated DFOS cables on both the
200 top and bottom longitudinal rib of each steel rebar. DFOS cables are installed on both sides of the
201 rebar to account for localised bar bending, as recommended by Poldon et al. (2022). The cables
202 were installed using the same procedure as described by Brault and Hoult (2019b), which includes:
203 (1) sanding the longitudinal rib smooth, (2) cleaning the rib with degreaser, water, and 99%
204 isopropyl alcohol, (3) gluing the cable to the longitudinal rib using a cyanoacrylate adhesive, and
205 (4) placing a 3-5 mm layer of silicone on top of the cable to protect it during concrete pouring.
206 Measurements were taken using a Luna ODiSi 6104 fibre optic analyzer with a gauge length of
207 2.6 mm and a sampling rate of 1 Hz.

208 Complementary to the distributed sensing technology, linear potentiometers were also used
209 to measure the displacement of the beams. Figure 1(b) shows the configuration of the linear
210 potentiometers, which were located at midspan and at each of the supports. This configuration
211 enables determination of the midspan beam deflection corrected for support settlement. Finally, a
212 load cell was connected to the hydraulic jack and was used to determine the load applied to the
213 beam. Data was collected from the load cell and linear potentiometers at a sampling rate of 1 Hz.

214 **2.4 Testing Procedure**

215 Figure 1(b) and (c) shows the test set up for the beam specimens, which were tested in three-point
216 bending in a self-reacting frame. The beam span was 1000 mm, with equal shear spans (a) of 500
217 mm and a shear span-to-effective depth ratio (a/d) of 4.0. Loading was applied using a hydraulic
218 cylinder at a rate of approximately 0.1 kN/s. Loading was paused at 5 kN increments throughout
219 each test to mark cracks. Cracks were marked on the side of the beam opposite to the side that was
220 analyzed with DIC. Steel plates measuring 12.6 mm thick and 100 mm along the length of the
221 beam were placed under the loading points and at the supports. The support condition at the west
222 end of the beam was roller, while the support at the east end of the beam was a pin (see Figure 1).

223 **3.0 Results and Discussion**

224 **3.1 Mechanical Behaviour**

225 Figure 2 summarizes the results of the mechanical testing of concrete with varying amounts of
226 GNP at 28 days after pouring with Figure 2(a) showing the normalized results of the compressive
227 strength testing. The normalized compressive strength shown in Figure 2(a) was calculated as the
228 compressive strength of each cylinder divided by the average strength of the control concrete
229 (without any GNP). In all cases the control concrete was cast on the same day using the same mix

230 design and raw ingredients. Despite having the same mix design, different batches casted on
231 different days with different environmental conditions can result in slightly different control
232 concrete strengths (Choo and Newman, 2003). Nevertheless, the GNP concrete normalized
233 strengths shown in Figure 2 were only normalized against control batches that were mixed at the
234 same time as the respective GNP concretes.

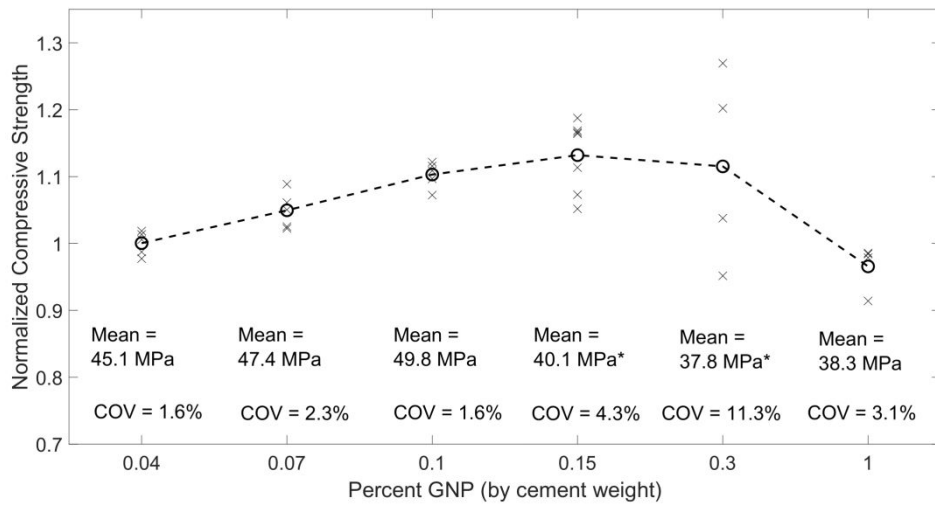
235 The results in Figure 2(a) do not show strength enhancements for GNP concentrations of 0.04 wt%
236 (by cement weight), but as the GNP concentration increased, the average compressive strengths
237 also increased. For GNP concentration of 0.07, 0.1, and 0.15 wt%, increases in average
238 compressive strength of 1.05, 1.10, and 1.14 times the control mix were observed. However, when
239 the concentration increased to 0.3 wt% GNP, the normalized average compressive strength
240 decreased to 1.12 and subsequently to 0.97 for a GNP concentration of 1 wt%.

241 Comparing the variability amongst the compressive strength of the tested cylinders (based
242 on 5 repeated tests), the results in Figure 2(a) show that most batches had coefficient of variations
243 (COV) below 4.3%, which is considered low for most concrete (Bentz et al., 2006). The exception
244 was the concrete with 0.3 wt% GNP content, which has a COV of 11.3% with two tests well above
245 the average (as high as 1.27) and two tests well below the average (as low as 0.95). These results
246 suggest that this GNP concentration was slightly above the optimal concentration of GNP. If
247 individual cylinders in the 0.3 wt% GNP concrete batch had more GNP than the other cylinders in
248 the batch, it is possible a steep decline in compressive strength could occur with increased
249 agglomeration associated with a higher GNP concentration (Jiang et al., 2023). This appears to be
250 the case for the 0.3 wt% GNP concrete as half the cylinders show normalized compressive strength
251 of above 1.2 while the other half show normalized compressive strengths below 1.04. This suggests
252 GNP dispersion is likely not even across an entire concrete volume resulting in variability in the

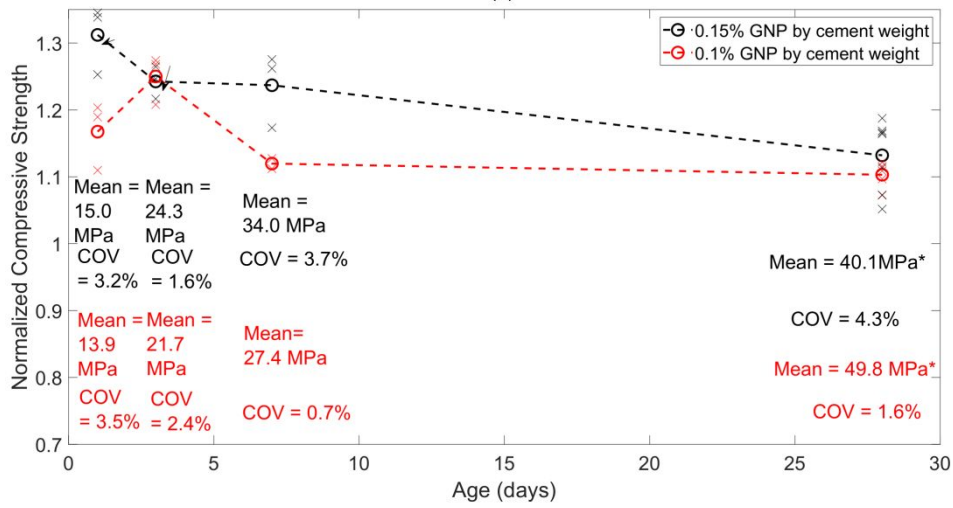
253 actual GNP concentration, highlighting the need of quality dispersion, especially at higher GNP
254 concentrations.

255

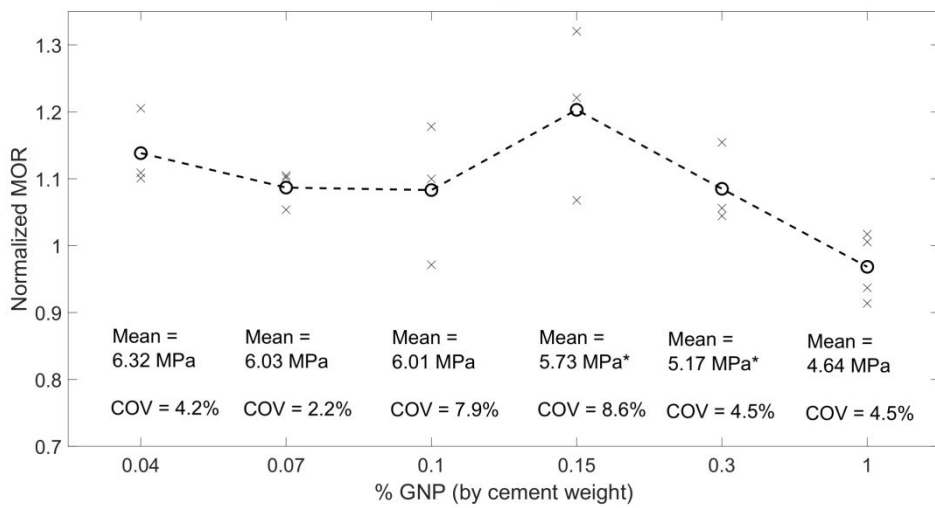
Draft



(a)



(b)



(c)

257

258 **Figure 2:** Mechanical properties: (a) 28-day normalized compressive strength for varying GNP

259 concentrations, (b) Time-dependent compressive strength of concrete with varying GNP

260 concentrations, (c) Modulus of rupture results for varying GNP concentrations tested at 28-days.

261 *These specimens were from different batches of concrete as the rest and had different control

262 strengths. The mix design remained the same but different batches with different environmental

263 conditions resulted in slightly different concrete strengths.

264 High GNP concentrations have been found in past research to result in strength reductions,

265 as large amounts of GNPs cause more agglomeration and thus, limited locations for nucleation

266 sites for hydration, which results in weak regions in the concrete (Jiang et al., 2023). The reported

267 optimal GNP concentration has also varied amongst past research. Studies by Chen et al., (2019),

268 Jiang et al. (2021), and Ismail et al., (2022) found the optimal concentration to be between 0.025

269 and 0.05 wt%, while Jaramillo and Kalfat (2023) found the optimal concentration to be between

270 0.2 and 0.25 wt%, which is similar to the observations in this study. This could be due to the

271 properties of the GNP used in each study, as optimum concentrations of 0.025 wt%-0.05 wt% were

272 associated with a lower surface area (between 100 and 300 m²/g) compared to the GNP used by

273 Jaramillo and Kalfat (2023) (536 m²/g) and in this study (363 m²/g). Another possible reason is

274 that the studies with the higher optimal GNP dosage also had low cement contents in the concrete

275 mix design (less than 350 kg/m³ cement) which may mean more GNP is required for efficient

276 particle packing in these mixes.

277 Figure 2(b) summarizes the time-dependent concrete compressive strength for GNP

278 concentrations of 0.1 wt% and 0.15 wt%, which correspond to the GNP concentrations that

279 represented the highest potential based on compressive testing at 28-days. Tests were conducted

280 at 1, 3, 7, and 28 days after pouring. The results in Figure 2(b) show that at early ages (1, 3, and 7
281 days), both tested GNP concentrations had higher normalized compressive strengths when
282 compared to at 28 days. More specifically, the concrete with a GNP concentration of 0.15 wt%
283 had 1.31 times higher compressive strength relative to the control 1 day after pouring, compared
284 to only 1.14 times higher after 28 days. Similarly, the concrete with a GNP concentration of 0.1
285 wt% had 1.25 times the compressive strength 3 days after pouring compared to only 1.10 times
286 after 28 days. A possible reason for the higher percentage increase in compressive strength at early
287 ages for GNP concrete is that higher amounts of weak and disorderly cement hydration crystals
288 exist at early ages in concrete. The GNPs can eliminate the disorderly crystals and organize the
289 hydration crystals into polyhedron type shapes which can be more tightly packed and result in
290 increased strength (Ming-li et al., 2016).

291 The higher compressive strength of the GNP concrete relative to the control decreases
292 significantly by day 7 (8% drop in in the 0.15 wt% GNP from day 1 and 13% drop in 0.1% GNP
293 from day 3). However, by 7 days there is typically enough strength gain from low cement concretes
294 on their own to resist dead loads in reinforced concrete structural elements (Hannesson et al.,
295 2012). A higher concrete compressive strength is important during construction at, or before three
296 days, as contractors aim to remove temporary formwork during that timeframe to construct the
297 next structural elements. Over the long-term, the higher compressive strength of the GNP concrete
298 could yield higher shear strength, flexural strengths, and anchorage of reinforcement. Thus, the
299 structural behaviour of reinforced concrete members with GNP concrete will be assessed in the
300 following sections.

301 In addition to compressive strength, the flexural strength of the GNP concrete was also
302 evaluated through four point bending tests on small-scale prisms. Figure 2(c) shows the modulus

303 of rupture (flexural strength) of the concrete with varying GNP concentrations 28 days after
304 pouring. The results show that for the concentrations of GNP tested, the enhancement in flexural
305 strength remained fairly constant (between 1.1 and 1.2 times higher than the control). These values
306 are comparable to the observations made by Jiang et al. (2021). The 0.04 wt% GNP concentration
307 had a modulus of rupture that was 1.14 times larger than the control, while the 0.07 wt% and 0.1
308 wt% GNP concentrations had a flexural strength that was 1.09 and 1.08 times higher than the
309 control, respectively. These observed enhancements in the flexural strength of the GNP concrete
310 could be attributed to the bridging effect of the GNPs (Jiang et al., 2021). The bridging effect is
311 the ability of GNP to cross nano-cracks, which slows the growth of those cracks (Jiang et al.,
312 2021). However, with small amounts of GNP concentrations (less than or equal to 0.1 wt% GNP),
313 the flexural strength enhancement is limited by its ability to fully strengthen the interfacial
314 transition zone (Jiang et al., 2021). Without sufficient GNP reinforcement, weak zones in the
315 interfacial transition zone may result in only small and relatively uniform improvements in flexural
316 strength over different GNP concentrations.

317 However, the concrete with a GNP concentration of 0.15 wt% had the largest observed
318 increase in flexural strength of 1.20 times the control. This is the same GNP concentration that
319 produced the maximum compressive strength enhancements, suggesting once again that for the
320 type of GNP used in this study, the optimal concentration is approximately 0.15 wt% by cement
321 weight. It is likely that the interfacial transition zone could be optimally strengthened with this
322 GNP concentration. Yet, for GNP concentrations beyond 0.15 wt%, the enhancements in flexural
323 strength declined to 1.08 and 0.97 for GNP concentrations of 0.3 and 1 wt%, respectively, as
324 agglomeration effects may be occurring at the higher concentrations. A GNP concentration of 1
325 wt% resulted in a decrease in the flexural strength relative to the control, (reaching 97% of the

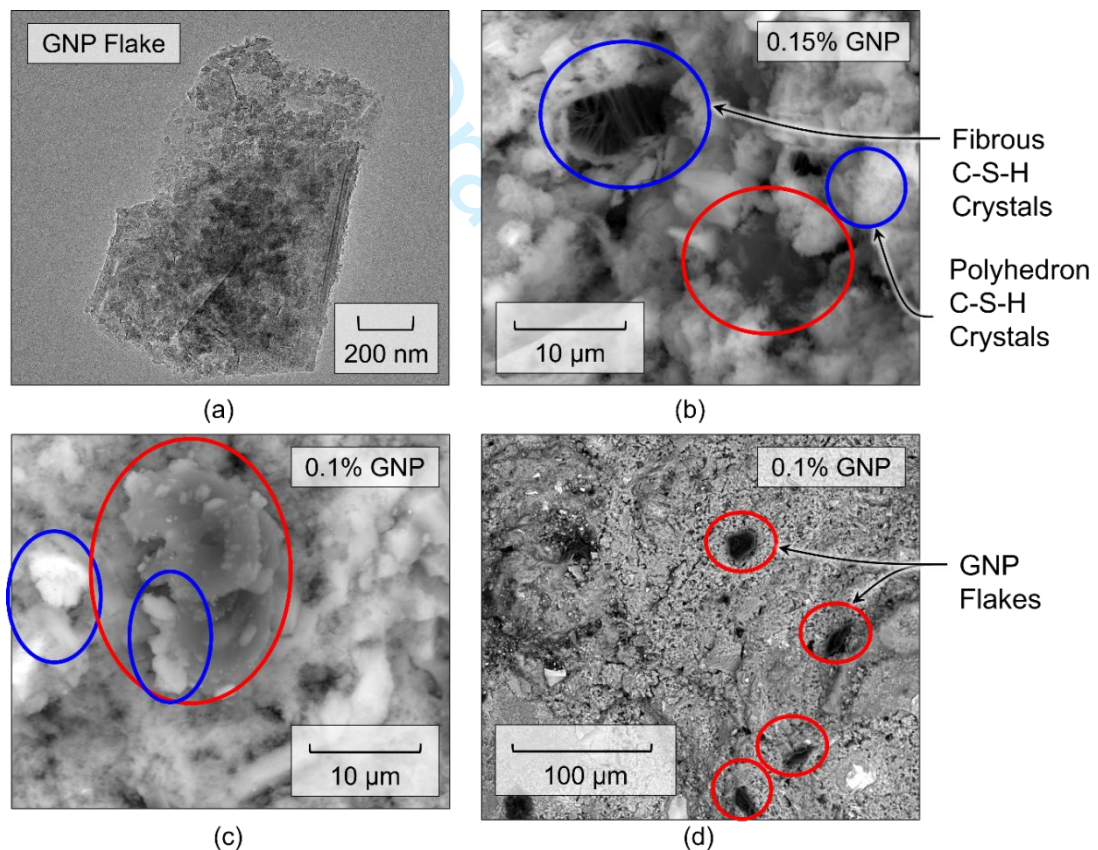
326 control modulus of rupture), suggesting once again that the addition of high concentrations of GNP
327 can actually be detrimental to the mechanical behaviour of the concrete.

328 To better understand the reasons for the observed enhancements in mechanical properties
329 of the GNP concrete, scanning electron microscopy (SEM) images were taken to examine the
330 dispersion of the GNPs and the microstructure of the material. A Quanta 250 environmental SEM
331 was used with an accelerated voltage of 20 kV and a working distance of 10.9 mm. Additional
332 information regarding the image acquisition procedure can be found in Haridas et al. (2024).
333 Figure 3 shows the SEM images of samples containing 0.1 wt% and 0.15 wt% GNPs, as well as a
334 transmission electron microscope (TEM) image of a representative GNP flake. Figure 6(a) shows
335 a single GNP flake that is approximately 1 μm wide, which represents an average size GNP flakes
336 observed in the concrete; these are visible as concentrated black dots in the SEM images. In the
337 SEM images (Figure 3 (b-d)), the largest GNP flakes are circled in red, while locations of calcium
338 silicate hydrate (C-S-H) crystals are circled in blue. Past research has hypothesized that the
339 addition of GNP to cementitious materials promote the formation of more regularly shaped C-S-
340 H crystals which enhances the mechanical properties of the concrete since they can be more
341 densely packed (Jiang et al., 2021). Figure 3(b) shows stacked GNP flakes, about 10 μm diameter,
342 near a polyhedron shaped C-S-H formation. However, in areas devoid of GNPs disorderly fibrous
343 crystals formed across a pore (i.e., an air void) in the concrete. This addition of GNPs helps limit
344 the amount of these weak fibrous crystals, thus promoting more of the polyhedron shaped
345 formations seen throughout Figure 3 (b) and (c). This more densely packed microstructure could
346 also explain the lower porosity of concrete with GNPs reported by other researchers (Meng and
347 Khayat, 2018). Figure 3(c) also shows stacked GNP flakes (18 μm diameter) in which individual

348 graphene layers are visible. Additionally, non fibrous (seen on the GNP flakes) C-S-H crystals are
 349 visible, which use these GNP flakes as a nucleation site.

350 Figure 3(d) shows the distribution of GNP flakes (sample containing 0.1 wt% GNP) within
 351 the concrete at a smaller magnification. The red circles in the image show the larger GNP
 352 aggregates (10-20 μm diameter), but smaller GNP flakes are also visible, which are the black,
 353 darker colored specks seen spaced throughout the concrete. This SEM image shows the wide
 354 distribution in particle size for the type of GNP used in this concrete as well as its effectiveness at
 355 dispersing throughout the concrete.

356



357

358 **Figure 3:** Images of GNPs and GNP concrete: a) TEM image of GNP flake b) SEM image of

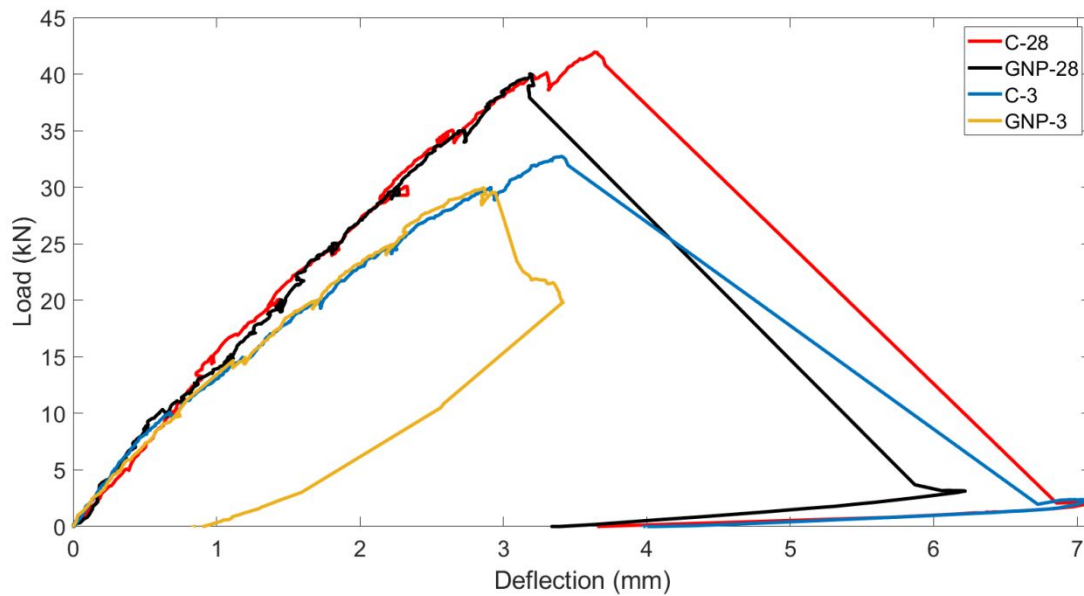
359 0.15 wt% GNP concrete, c) SEM image 0.1 wt% GNP concrete showing GNP flakes and

360 calcium silicate hydrate crystals, d) low magnification SEM image of 0.1 wt% GNP concrete.
361 GNP flakes are circled in red and calcium silicate hydrate (C-S-H) crystals are circled in blue

362 **3.2 Structural Behaviour**

363 *Load-Deflection Response*

364 Based on the mechanical properties of GNP concrete tested in this study, it was determined that a
365 GNP concentration of 0.15 wt% provided the highest benefits in terms of compressive and tensile
366 strength. To investigate the implications that these enhancements in mechanical properties could
367 have on the structural behaviour of reinforced concrete, beams fabricated of concrete with a GNP
368 concentration of 0.15 wt% were tested in three-point bending at 3 and 28 days after casting and
369 compared to concrete beams without the addition of GNPs. Figure 4 shows the load versus midspan
370 deflection of each of the four beams tested in this study and Table 4 summarizes the compressive
371 strength of the concrete on the day of testing as well as key structural response parameters for each
372 beam, including the cracked stiffness (K_i), ultimate load carrying capacity (P_u), and the ultimate
373 displacement (Δ_u). It is noted that the crack stiffness was taken as the stiffness of the beams
374 between a load of 15 and 25 kN.



375

376

Figure 4: Load deflection behaviour

377

Table 4: Structural response parameters for reinforced concrete beams

Beam Name	Age at Testing (Days)	f'_c (MPa)	$K_{cracked}$ (kN/mm)	P_u (kN)	$P_{u,predicted}$ (kN)	Δ_u (mm)
C-3	3	19.5	10.0	32.7	29.2	3.41
GNP-3	3	24.3	10.1	29.9	32.6	2.86
C-28	28	37.6	11.5	41.9	40.6	3.64
GNP-28	28	41.2	14.2	40.0	42.5	3.19

378 The results in Figure 4 and Table 4 show that, as expected, the beams tested 3 days after casting

379 had lower cracked stiffness and ultimate load carrying capacities when compared with the beams

380 tested at 28-days after casting. Both concrete types at this age had lower compressive strength, and

381 since compressive strength is related to the elastic modulus and cracking strength of the concrete,

382 it was expected that these beams would have a lower stiffness and strength. According to CSA

383 A23.3 (2019), the predicted shear capacities (labelled as $P_{u,predicted}$ in Table 4) for the early age

384 specimens with lower compressive strengths were approximately 0.75 times that of the 28-day

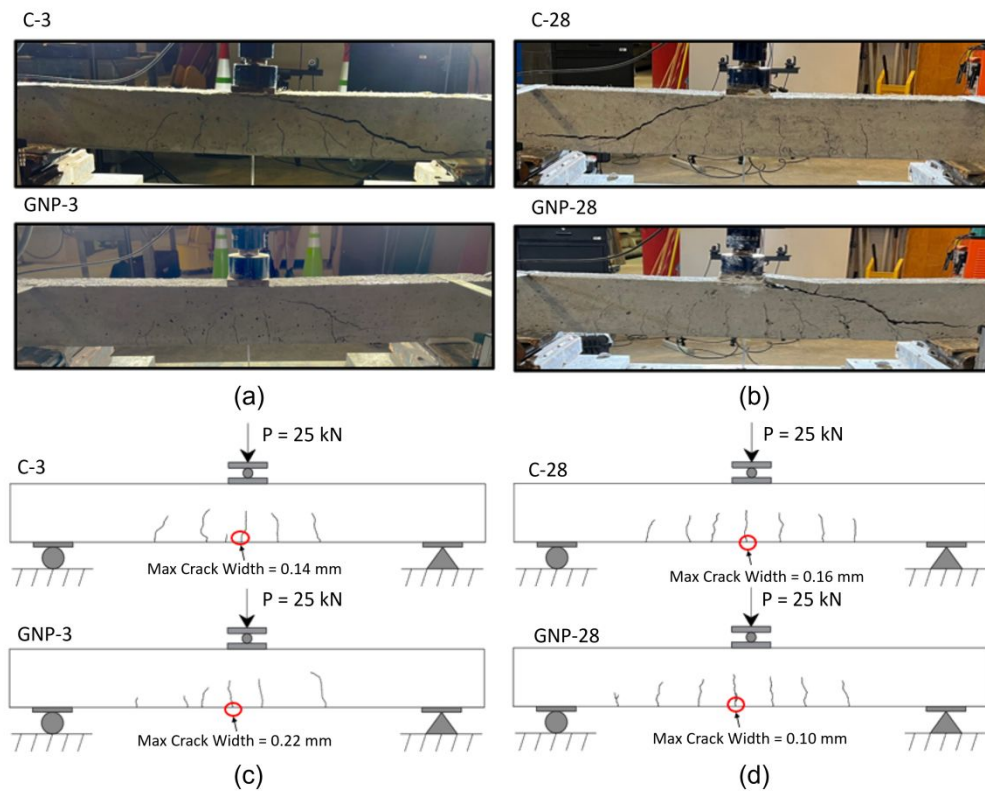
385 specimens and the experimental results generally agreed with those predictions.

386 The control beam specimens (without GNPs) had load carrying capacities that were 1.09
387 and 1.05 times larger than the beams with GNP. As expected, all the beams failed in shear and
388 Figure 5(a) shows the crack distributions at failure. Even though the GNP concrete had a higher
389 compressive strength, and thus should have had a higher concrete shear strength (2-3 kN higher
390 according to CSA A23.3 (2019) predictions), the beams fabricated from concrete with GNP had
391 lower shear capacities. Since the differences in ultimate capacity and compressive strength were
392 small, it is possible that the difference in ultimate capacity could be due to normal variance in
393 shear strength since shear behaviour in reinforced concrete especially without shear reinforcement
394 is inherently variable (Sykora et al., 2018). Nevertheless, these results suggest that further research
395 is required to better understand how the presence of GNPs affects the shear strength of reinforced
396 concrete structural elements.

397

398

Draft



399

400 **Figure 5:** Failure modes and crack patterns of beams: (a) C-3 versus GNP-3 failure modes, (b)

401 C-28 versus GNP-28 failure modes, (c) C-3 versus GNP-3 crack patterns, (d) C-28 versus GNP-

402 28 crack patterns

403 ***Shrinkage Behaviour***

404 Using DFOS, it is possible to measure restrained concrete shrinkage by examining the strains along

405 the steel reinforcement prior to loading the concrete beams. Shrinkage is a time dependent material

406 property of concrete in which a concrete member experiences an overall volume reduction during

407 the curing process (Neville, 2011). Because of the presence of the reinforcing steel in the beams,

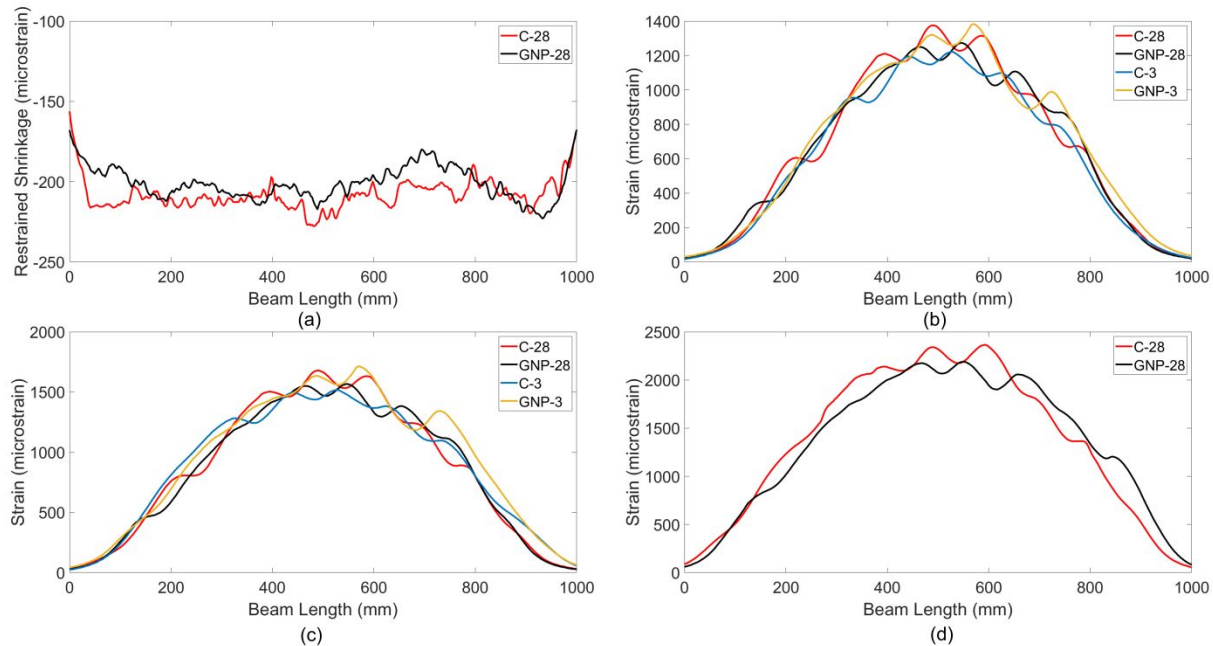
408 the concrete shrinkage is restrained by the reinforcement, meaning initially the reinforcement is in

409 compression (Poldon et al., 2022). Excessive shrinkage and subsequent restraint of the shrinkage

410 can cause cracking of concrete prior to any applied loading. As concrete mix designs become more
411 complex, including the use of advanced additives like GNPs, there is a need to study the shrinkage
412 behaviour of concrete to ensure that traditional assumptions used in structural design remain
413 appropriate. Figure 6(a) shows the strain distributions along the steel reinforcement just prior to
414 loading of the beam (on day 28). This measurement includes an adjustment for temperature as
415 differences in temperature will result in thermal expansion/contraction strains along the fibre. This
416 approach to measuring restrained shrinkage in concrete is further described by Yager et al. (2022b).

417 Figure 6(a) shows the restrained shrinkage of the two beams (one with GNP and one
418 without) at 28 days after casting. The results show that both beams had a relatively constant
419 restrained shrinkage of approximately -200 microstrain. Past studies have found that the amount
420 of restrained shrinkage can vary significantly depending on the concrete mix design, however, it
421 typically will range between -100 to -400 microstrain at 28 days (Bado et al., 2021). These results
422 suggests that the addition of the GNPs into the concrete mix design had little-to-no effect on the
423 shrinkage behaviour of the concrete. This is a positive result, as excessive shrinkage can cause
424 serviceability concerns in reinforced concrete structures, including shrinkage cracking.

425



426

427 **Figure 6:** DFOS strain measurements: (a) Restrainted shrinkage measured at 28 days, (b) Beam
 428 strains along the steel reinforcement at service ($P = 25$ kN), (c) Reinforcement strains at 30 kN
 429 (near ultimate load for C-3 and GNP-3), (d) Reinforcement strains 40 kN (near ultimate load for
 430 beams C-28 and GNP-28).

431 *Strain and Cracking Behaviour*

432 Figure 6(b) shows the strain distributions along the length of the steel reinforcement from support
 433 to support (i.e., the 1 m span) for each of the specimens at the service load, which was assumed to
 434 be ~60% of expected yield load, which corresponds to a point load (P) of 25 kN. The results are
 435 the average of the strain along the top and bottom fibre optic cables, to remove any localized bar
 436 bending from the results. The peaks in the distributions are the locations of cracks, which cause
 437 localized tensile demand in the steel reinforcement. Comparing the strain distributions amongst
 438 the tested beams there exists minimal difference in the results and the peak strains are within

439 approximately 160 microstrain of one another. Small differences in the maximum strains may be
440 due to the widths of the cracks that formed at midspan.

441 Figure 5(b) shows the crack pattern as well as the location and magnitude of the maximum
442 crack width for each beam (measured using DIC) at the 25 kN service load. Beam GNP-3 had the
443 highest maximum crack width (0.22 mm), followed by C-28, C-3, and GNP-28, which had
444 maximum crack widths of 0.16 mm, 0.14 mm, and 0.10 mm at 25 kN. Maximum strains in the
445 steel reinforcement also followed the same pattern. This pattern was evident for the entire test after
446 the cracking load. Because there was no apparent pattern as to which beams had wider crack widths
447 and higher strains (between control and GNP concrete), this suggests that crack width formation
448 was not influenced by the presence of the GNPs. Furthermore, as shown in Figure 5(b), the
449 distribution of cracks along the length of the beam were similar for beams tested at the same age,
450 which suggests further the presence of the GNPs in the concrete had no discernable effect on the
451 cracking behaviour.

452 The results in Figure 5(b) also show that near the supports on the left side of the beams, and on the
453 right side for C-3, the beams tested at 3-days had lower strains when compared with the beams
454 tested at 28-days. In Figure 6(b), the results show that these regions were uncracked during testing
455 for the beams tested at 3-days, while the regions over which cracks extended along the length of
456 the beam were longer for the beams tested at 28-days. Cracking that extended towards the supports
457 are likely the reason for the higher strains in these regions. The appearance of fewer cracks near
458 the supports for the beams tested at 3-days is due to the fact that early age concrete can have up to
459 2.5 times the tension stiffening capacity when compared to the same concrete at 28-days after
460 casting (Bentz, 2000), meaning cracks form at higher moments for these specimens. However,
461 GNP-3 had higher strains on the right side of the beam. This could be explained by the fact that at

462 25 kN, GNP-3 may have had higher shear strains on the right side and thus higher longitudinal
463 reinforcement strain contributions from shear, as observed by Poldon et al. (2022). This is
464 evidenced by the inclination of the rightmost crack in GNP-3 (seen in Figure 6(b)). Since GNP-3
465 failed only 5 kN later, the shear strains were higher than C-3 which failed 8 kN later.

466 Figure 6(c) and (d) show the strain distributions along the steel reinforcement close to the
467 ultimate loads for both the beams tested at 3-days ($P = 30$ kN) and 28-days ($P = 40$ kN). At a point
468 load of 30 kN, GNP-3 was about to fail and thus had higher strains on the right side of the beam
469 (within 250 mm of the support). C-3, which was within 3 kN from its failure load had higher shear
470 strains within 150 mm of the right support. At 40 kN, the beams tested 3-days after casting had
471 already failed. GNP-28 had higher strains on the right side of the beam as it was very close to
472 failure. At this load, C-28 was within 2 kN from failing and had slightly higher strains on the left
473 side of the beam, which is the side of the beam that eventually failure in shear. Aside from GNP-
474 3, none of these higher strains due to shear, were observed at the service load ($P = 25$ kN). Overall,
475 even though the use of DFOS can provide unprecedented insight into the behaviour of reinforced
476 concrete elements, the observed differences in behaviour between the control and GNP concrete
477 beams were small. Further investigation into large scale members and on additional mechanical
478 properties, such as elastic modulus, should be undertaken to determine the full benefits of GNP on
479 structural behaviour.

480 **4. Conclusions**

481 This paper investigated the effects of adding GNPs produced by a novel process to low cement
482 concrete, specifically examining the influence that the GNPs had on the time-dependent
483 compressive strength and flexural strength through cylinder and modulus of rupture tests. The
484 study also examined the structural behaviour of small-scale reinforced concrete beams tested

485 under three-point bending at both 3 and 28 days after casting. The following specific conclusions
486 were drawn from this study:

- 487 1. The optimal GNP concentration was found to be between 0.15 wt% and 0.3 wt% of cement,
488 as the 0.15 wt% GNP concrete produced the highest compressive strength at 28 days that was
489 1.14 times higher than the control mix, as well as flexural strength, which was 1.20 times
490 higher than the control mix. These results are comparable to work by Jaramillo and Kalfat
491 (2023), who suggested an optimal GNP concentration of 0.2-0.25 wt%;
- 492 2. Concrete with a 0.15 wt% GNP concentration in cement had a compressive strength that was
493 up to 1.31 times larger than the control at 1 day after pouring, suggesting that the use of GNPs
494 can enhance the early age strength of low cement concrete;
- 495 3. For GNP a concentration of 1 wt%, a decrease in the mechanical properties (compressive and
496 flexural strength) of the concrete was observed;
- 497 4. The restrained shrinkage behaviour of GNP concrete using DFOS was not significantly
498 different to the control mix; both mixes experienced restrained shrinkage strains of -200
499 microstrain, suggesting the addition of GNPs to the concrete mix did not change the shrinkage
500 behaviour of the concrete;
- 501 5. The structural behaviour of beams cast with concrete with a 0.15 wt% GNP concentration was
502 similar to the control beams for specimens tested at the same age, including comparable
503 stiffness, reinforcement strain behaviour, crack patterns, and crack widths; and
- 504 6. The ultimate capacity of the control beams (without GNPs) were 10% and 5% higher than the
505 beams consisting of GNP concrete, suggesting limited advantages to the overall structural
506 behaviour of reinforced concrete with the addition of GNPs.

507 Ultimately, the observed benefits with respect to the mechanical properties of concrete with GNP
508 suggest the potential for this material to be used as a strength enhancing additive; however, no
509 significant differences were observed with respect to structural behaviour based on a limited
510 sample set. Thus, further research on large scale GNP reinforced concrete structural members
511 should be performed to fully understand the implications of using GNP as an admixture at scale.

512 **Acknowledgements**

513 The authors would like to thank the Natural Sciences and Engineering Research Council of
514 Canada (NSERC), the Technology Development Pilot Fund by Queen's Partnerships and
515 Innovation (QPI) and a Smith Engineering Dean's research Fund for providing funding for this
516 project. The authors would also like to thank Jenna Cherepacha for their technical support in this
517 research.

518 **Competing Interests Statement**

519 Competing interests: The authors declare there are no competing interests.

520 **Data Availability Statement**

521 Data generated or analyzed during this study are available from the corresponding author upon
522 reasonable request.

523 **References**

524 Abedi, M., Fangueiro, R., & Gomes Correia, A. (2020). Ultra-sensitive affordable cementitious
525 composite with high mechanical and microstructural performances by hybrid CNT/GNP.
526 *Materials*, 13(16), 3484.

- 527 Adesina, A. (2020). Recent advances in the concrete industry to reduce its carbon dioxide
528 emissions. *Environmental Challenges*, 1, 100004.
- 529 Al-Dahawi, A., Öztürk, O., Emami, F., Yıldırım, G., & Şahmaran, M. (2016). Effect of mixing
530 methods on the electrical properties of cementitious composites incorporating different carbon-
531 based materials. *Construction and Building Materials*, 104, 160-168.
- 532 ASTM A370, 2023, Standard Test Methods and Definitions for Mechanical Testing of Steel
533 Products. ASTM International: West Conshohocken, PA.
- 534 ASTM C39, 2021, Standard Test Method for Compressive Strength of Cylindrical Concrete
535 Specimens. ASTM International: West Conshohocken, PA.
- 536 ASTM C78, 2022, Standard Test Method for Flexural Strength of Concrete (Using Simple Beam
537 with Third-Point Loading). ASTM International: West Conshohocken, PA.
- 538 Bado, M. F., Casas, J. R., Dey, A., Berrocal, C. G., Kaklauskas, G., Fernandez, I., & Rempling,
539 R. (2021). Characterization of concrete shrinkage induced strains in internally-restrained RC
540 structures by distributed optical fiber sensing. *Cement and Concrete Composites*, 120, 104058.
- 541 Bentz, E. C. (2000). Sectional analysis of reinforced concrete members. Toronto: University of
542 Toronto.
- 543 Bentz, E. C., Vecchio, F. J., & Collins, M. P. (2006). Simplified modified compression field
544 theory for calculating shear strength of reinforced concrete elements. *ACI structural journal*,
545 103(4), 614-624.
- 546 Brault, A., & Hoult, N. (2019a). Monitoring reinforced concrete serviceability performance
547 using fiber-optic sensors. *ACI Structural Journal*, 116(1), 57-70.

- 548 Brault, A., & Hoult, N. (2019b). Distributed reinforcement strains: measurement and application.
549 *ACI Structural Journal*, 116(4), 115-127.
- 550 Chaudhury, R., Sharma, U., Thapliyal, P. C., & Singh, L. P. (2023). Low-CO₂ emission
551 strategies to achieve net zero target in cement sector. *Journal of Cleaner Production*, 137466.
- 552 Cheaptubes (2023). Graphene Nanoplatelets Products, [https://www.Cheaptubes.Com/Product-](https://www.Cheaptubes.Com/Product-Category/Graphene-Nanoplatelets/)
553 [Category/Graphene-Nanoplatelets/](https://www.Cheaptubes.Com/Product-Category/Graphene-Nanoplatelets/).
- 554 Chen, G., Yang, M., Xu, L., Zhang, Y., & Wang, Y. (2019). Graphene nanoplatelets impact on
555 concrete in improving freeze-thaw resistance. *Applied Sciences*, 9(17), 3582.
- 556 Choo, B. S., & Newman, J. (2003). *Advanced Concrete Technology. processes*. Butterworth-
557 Heinemann.
- 558 Correlated Solutions Inc. (2023). Vic-3D. Correlated Solutions Digital Image Correlation,
559 <https://www.correlatedsolutions.com/vic-3d>.
- 560 Dai Pang, S., Gao, H. J., Xu, C., Quek, S. T., & Du, H. (2014). Strain and damage self-sensing
561 cement composites with conductive graphene nanoplatelet. *Sensors and Smart Structures*
562 *Technologies for Civil, Mechanical, and Aerospace Systems*, 2014, 9061, 546-556.
- 563 Dimov, D., Amit, I., Gorrie, O., Barnes, M. D., Townsend, N. J., Neves, A. I., Withers, F.,
564 Russo, S., & Craciun, M. F. (2018). Ultrahigh performance nanoengineered graphene–concrete
565 composites for multifunctional applications. *Advanced functional materials*, 28(23), 1705183.
- 566 Divya, S., Praveenkumar, S., Akthar, A. S., & Karthiksundar, N. (2023). Performance variation
567 of graphene nanoplatelets reinforced concrete concerning dispersion time. *Materials Today:*
568 *Proceedings*.

- 569 Du, H., & Dai Pang, S. (2015). Enhancement of barrier properties of cement mortar with
570 graphene nanoplatelet. *Cement and Concrete Research*, 76, 10-19.
- 571 Du, H., Gao, H. J., & Dai Pang, S. (2016). Improvement in concrete resistance against water and
572 chloride ingress by adding graphene nanoplatelet. *Cement and Concrete Research*, 83, 114-123.
- 573 Fayyad, T. M., & Lees, J. M. (2014). Application of digital image correlation to reinforced
574 concrete fracture. *Procedia Materials Science*, 3, 1585-1590.
- 575 Hannesson, G., Kuder, K., Shogren, R., & Lehman, D. (2012). The influence of high volume of
576 fly ash and slag on the compressive strength of self-consolidating concrete. *Construction and*
577 *Building Materials*, 30, 161-168.
- 578 Haridas, H., Kader, A. K. A., Sellathurai, A., Barz, D. P., & Kontopoulou, M. (2024).
579 Noncovalent functionalization of graphene nanoplatelets and their applications in
580 supercapacitors. *ACS Applied Materials & Interfaces*, 16(13), 16630-16640.
- 581 Hoult, N. A., Dutton, M., Hoag, A., & Take, W. A. (2016). Measuring crack movement in
582 reinforced concrete using digital image correlation: Overview and application to shear slip
583 measurements. *Proceedings of the IEEE*, 104(8), 1561-1574.
- 584 Ismail, F. I., Farhan, S. A., Husna, N., Shafiq, N., Wahab, M. M. A., & Abd Razak, S. N. (2021).
585 Influence of graphene nanoplatelets on the compressive and split tensile strengths of geopolymers
586 concrete. *IOP Conference Series: Earth and Environmental Science*, 945, 012060.
- 587 Ismail, F. I., Shafiq, N., Abbas, Y. M., Bheel, N., Benjeddou, O., Ahmad, M., & Sabri, M. M.
588 (2022). Behavioral assessment of graphene nanoplatelets reinforced concrete beams by

- 589 experimental, statistical, and analytical methods. *Case Studies in Construction Materials*, 17,
590 e01676.
- 591 Jaramillo, L. J., & Kalfat, R. (2023). Fresh and hardened performance of concrete enhanced with
592 graphene nanoplatelets (GNPs). *Journal of Building Engineering*, 106945.
- 593 Jiang, Z., Sevim, O., & Ozbulut, O. E. (2021). Mechanical properties of graphene nanoplatelets-
594 reinforced concrete prepared with different dispersion techniques. *Construction and Building*
595 *Materials*, 303, 124472.
- 596 Kim, K., Shin, M., & Cha, S. (2013). Combined effects of recycled aggregate and fly ash
597 towards concrete sustainability. *Construction and Building Materials*, 48, 499-507.
- 598 Mardlin, K., Osazuwa, O., & Kontopoulou, M. (2022). Solvent-free thermomechanical
599 exfoliation of graphite into graphene nanoplatelet flakes: Implications for conductive
600 composites. *ACS Applied Nano Materials*, 5(4), 4938-4947.
- 601 Masoudi, A., & Newson, T. P. (2016). Contributed review: Distributed optical fibre dynamic
602 strain sensing. *Review of scientific instruments*, 87(1).
- 603 Meng, W., & Khayat, K. H. (2018). Effect of graphite nanoplatelets and carbon nanofibers on
604 rheology, hydration, shrinkage, mechanical properties, and microstructure of UHPC. *Cement and*
605 *Concrete Research*, 105, 64-71.
- 606 Poldon, J. J., Bentz, E. C., & Hoult, N. A. (2022). Assessing beam shear behavior with
607 distributed longitudinal strains. *Structural Concrete*, 23(3), 1555-1571.

- 608 Sahu, A., & Shanmugapriya, S. (2022). Overview of the Challenges in the Construction of
609 Multistorey Reinforced Concrete Structure. *International Journal of Engineering Trends and*
610 *Technology*, 70(7), 212-219.
- 611 Sevim, O., Jiang, Z., & Ozbulut, O. E. (2022). Effects of graphene nanoplatelets type on self-
612 sensing properties of cement mortar composites. *Construction and Building Materials*, 359,
613 129488.
- 614 Soutsos, M., Hatzitheodorou, A., Kanavaris, F., & Kwasny, J. (2017). Effect of temperature on
615 the strength development of mortar mixes with GGBS and fly ash. *Magazine of Concrete*
616 *Research*, 69(15), 787-801.
- 617 Sykora, M., Krejsa, J., Mlcoch, J., Prieto, M., & Tanner, P. (2018). Uncertainty in shear
618 resistance models of reinforced concrete beams according to fib MC2010. *Structural Concrete*,
619 19(1), 284-295.
- 620 Tong, T., Fan, Z., Liu, Q., Wang, S., Tan, S., & Yu, Q. (2016). Investigation of the effects of
621 graphene and graphene oxide nanoplatelets on the micro-and macro-properties of cementitious
622 materials. *Construction and Building Materials*, 106, 102-114.
- 623 Villalba, S., & Casas, J. R. (2013). Application of optical fiber distributed sensing to health
624 monitoring of concrete structures. *Mechanical Systems and Signal Processing*, 39(1-2), 441-451.
- 625 Wang, B., & Pang, B. (2019). Mechanical property and toughening mechanism of water
626 reducing agents modified graphene nanoplatelets reinforced cement composites. *Construction*
627 *and Building Materials*, 226, 699-711.

- 628 Wang, B., Jiang, R., & Wu, Z. (2016). Investigation of the mechanical properties and
629 microstructure of graphene nanoplatelet-cement composite. *Nanomaterials*, 6(11), 200.
- 630 Yager, J., Hoult, N. A., & Bentz, E. (2021). Evaluating the behaviour of functionally graded
631 reinforced concrete without transverse reinforcement using distributed sensing. *Construction and*
632 *Building Materials*, 295, 123612.
- 633 Yager, J., Hoult, N. A., Bentz, E. C., & Woods, J. (2022a). Shear-critical deep beams with
634 embedded functionally graded concrete struts. *ACI Structural Journal*, 119(6), 245-257.
- 635 Yager, J. S., Hoult, N. A., Bentz, E. C., & Woods, J. E. (2022b). Measurement of Restrained and
636 Unrestrained Shrinkage of Reinforced Concrete Using Distributed Fibre Optic Sensors. *Sensors*,
637 22(23), 9397.
- 638 Zhang, Y., Cui, M., Chen, G., & Han, W. (2022). Experimental study of the effects of graphene
639 nanoplatelets on microstructure and compressive properties of concrete under chloride ion
640 corrosion. *Construction and Building Materials*, 360, 129564.
- 641 Zhang, Y., Wang, Y., Yang, M., Wang, H., Chen, G., & Zheng, S. (2021). Effect of graphene
642 nanoplatelet on the carbonation depth of concrete under changing climate conditions. *Applied*
643 *Sciences*, 11(19), 9265.